

SUPPRESSING THE VORTEX-INDUCED VIBRATION OF A BRIDGE DECK VIA SUCTION

Shibo Tao^{1,2*} - Aiping Tang^{1,2} - Ketong Liu³

¹ Key Lab of Structures Dynamic Behavior and Control (Harbin Institute of Technology), Ministry of Education, Heilongjiang, Harbin, 150090, China

² School of Civil Engineering, Harbin Institute of Technology, Harbin 150090, China

³ College of Architecture and Civil Engineering, Xi'an University of Science and Technology, Xi'an, 710054, China

ARTICLE INFO

Article history:

Received: 27.6.2015.

Received in revised form: 26.11.2015.

Accepted: 1.12.2015.

Keywords:

Suction control

Vortex-induced vibration

Long span bridge

Bridge decks

Wind tunnel experiments

Numerical simulation

Aerodynamic stability

Abstract:

This paper presents experimental and numerical study with the objective of exploring the effect of suction control on vortex-induced vibration (VIV) of a bridge deck. The vertical and torsional responses of the model with or without suction control during this experiment were measured. The results demonstrate that the suction decreases the vibration amplitudes. The suction holes arranged on the undersurface near the leeward of the model has the best effect. To study the mechanism of the suction control, the aerodynamic stability of the model is analysed by the forced vibration method. The results demonstrate that the aerodynamic stability of the model is increased by the suction control.

1. Introduction

Long span bridges have recently been attracting increasing popularity for their structural shape, efficient use of materials and other optimal solutions [1-2]. Over the past several decades, the bridge span lengths have increased significantly [3]. As the span of bridges has increased, they show a higher sensitivity to wind excitation. Therefore, wind loading becomes one of the important factors that needs due consideration in design [4-5]. The vortex-induced vibration (VIV), especially at lock-in, is a phenomenon in which the vibration of a bridge immersed in a fluid flow is governed by the shedding of vortices from its surface. Although the VIV is self-limiting, it frequently occurs in long span bridges at low wind speeds. This may result in noise, strain the fatigue life of structures and even lead to disastrous structural damage, for example, the vortex-induced first-mode vibration of the Trans-Tokyo Bay Bridge

peaks at a wind velocity of approximately 16m/s, with a maximum amplitude exceeding 50 cm [6]. The VIV of the Great Belt East Bridge occurs at moderate wind speeds of approximately 5 m/s-10 m/s [7]. These issues have attracted the interest of many researchers over the years, and great efforts have been made to attenuate or suppress the phenomenon [8-11].

Flow control is broadly classified as passive and active control [12]. Passive control requires no auxiliary power and no control loop [13-14]. Larsen et al. [7] showed the effect of guide vanes to mitigate vortex shedding. The VIV of the Great Belt East Bridge was mitigated by fitting guide vanes at joints of the horizontal bottom plate and lower side panels of the box girders. Active control requires energy expenditure. Suction control is a type of active control methods. It has long been used to suppress flow separation [15]. In 1904, Prandtl [16] used suction to delay the boundary-layer separation from

* Corresponding author. Tel.: +8618745030417;
E-mail address: taoshibo1985@163.com.

the surface of a cylinder. Muralidharan et al. [17] designed a suction control strategy for a circular cylinder and implemented to assess its efficacy. Arcas and Redekopp [18] controlled wake vortex through base suction. Chng et al. [19] suppressed the flow separation of airfoils via suction. Xin et al. [20] conducted numerical simulations to analyse the efficiency of suction for increasing flutter stability of long-span bridges.

This paper presents experimental and numerical simulations for investigation of suction control for suppressing the vortex vibration in long-span bridges.

2. Experimental set-up

This experiment was performed in a wind tunnel at Harbin Institute of Technology in China (see Fig. 1). The wind tunnel is a closed circuit design with recirculated air. It has a 4 m (width) \times 3 m (height) \times 25 m (length) rectangular test section. The maximum

wind velocity is 45 m/s, the turbulence intensity of the free stream is less than 0.46% and the non-uniformity of the free stream is less than 1%. The free stream velocity (U) is measured by a precision propeller anemometer.

The dimensions of the 1:40 scale model of Great Belt East Bridge [22] deck section are given in Fig. 2. The model is 775 mm wide (B), 110 mm deep (D) and 1200 mm long (L), see Fig. 2 (a). The mass of the bridge model is 11 kg.

There are twenty-eight suction holes arranged on the undersurface of the model as shown in Figs. 2 (b) and 2 (c). The diameter of the suction hole (r_s) is 7 mm. As shown in Fig. 2(c), from the windward edge to the leeward edge, there are seven suction configurations, defined respectively as $K_1, K_2, K_3, K_4, K_5, K_6$ and K_7 . In each line, there are four suction holes. When the holes of one line are open, the others are sealed. This is one of the seven suction configurations. For convenience, we defined the K_0 suction configuration to represent the no control state.

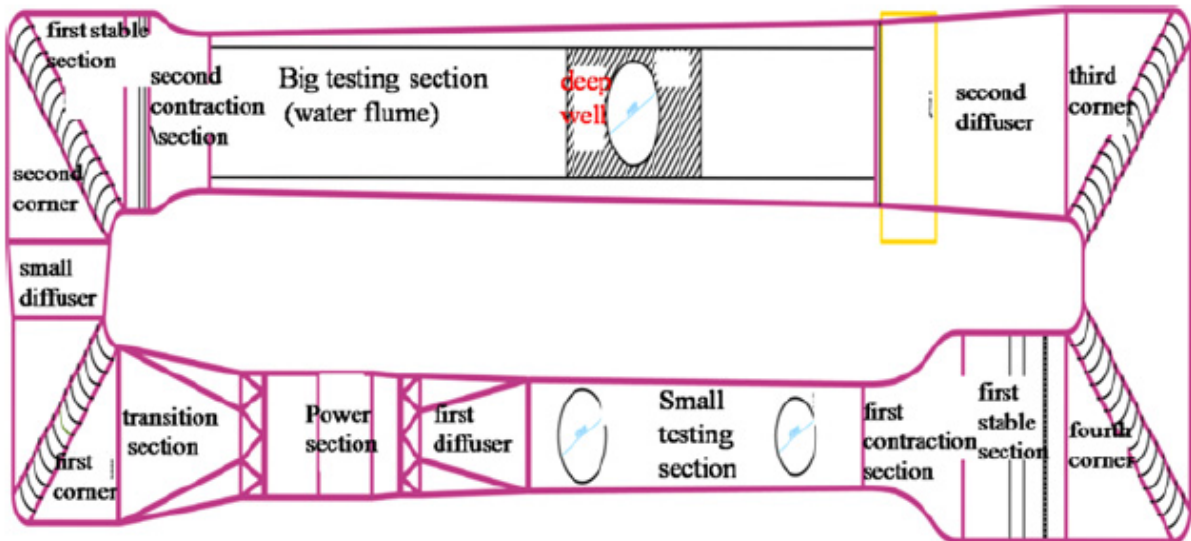
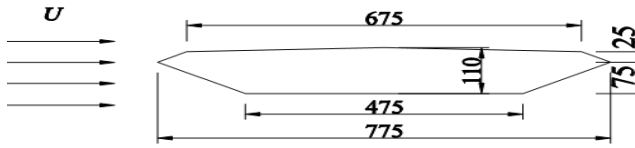
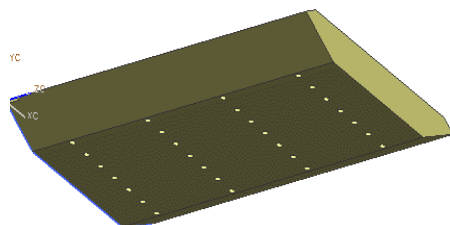


Figure 1. Sketch of the wind tunnel [21].

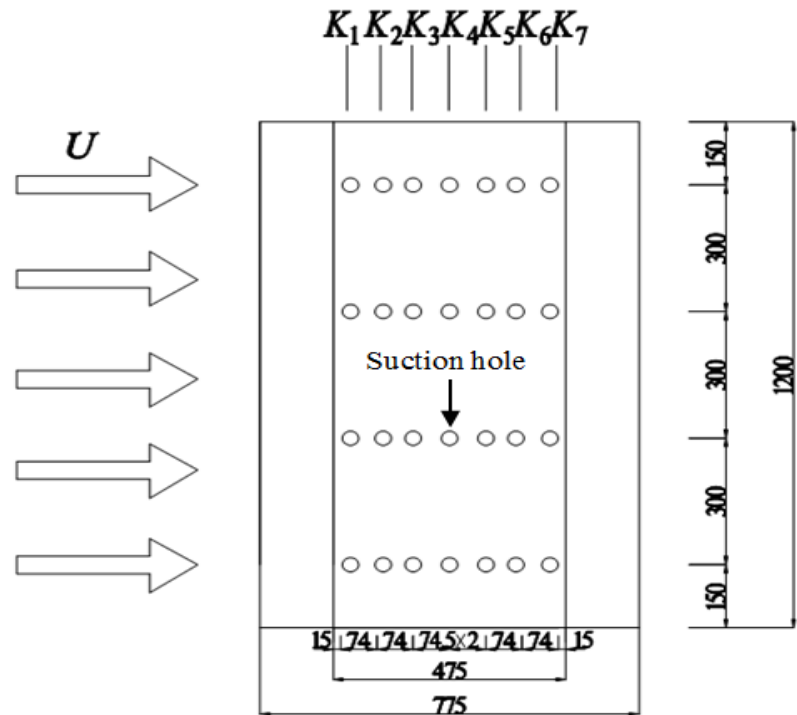


(a) The size of the model (millimetres)



(b) Schematic of the model

Figure 2. Bridge model.



(c) Bottom view of the model

Figure 2. Bridge model (continued).

The pneumatic circuit of the suction device is presented in Fig. 3, where: 1 - Vacuum pump, 2 - Gas tank, 3 - Magnetic exchange valve, 4 - Vacuum

filter, 5 - Vacuum reducer valve, 6 - Main pipe, 7 - Flow meter, 8 - Throttle valve, 9 - Branch pipe and 10 - Suction port.

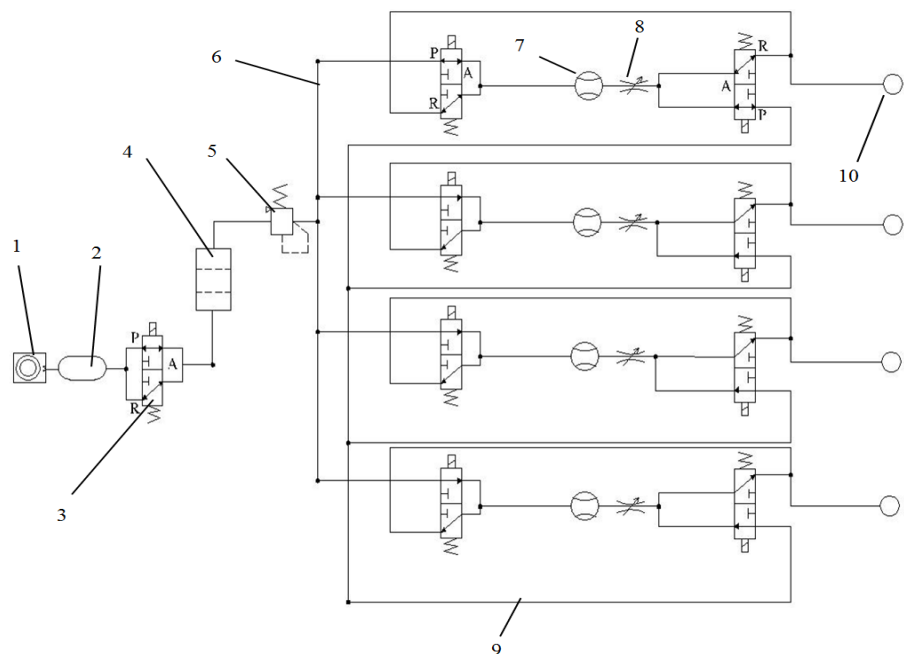


Figure 3. Pneumatic circuit of suction device.

The experimental facility is shown in Fig. 4. The stiffness of the individual coil springs was 1050 N/m and attached symmetrically on the lever arms. The spacing between these two coil springs is 490mm. The vertical natural frequency and the vertical damping ratio in still air were 4.7 Hz and 0.06% respectively. On the other hand, the torsional natural frequency and the torsional damping ratio in still air were 5.7Hz and 0.1%. Two end plates were used to foster a bidimensional flow. The blockage ratio of the whole system is about 3% and no attempt was made to correct the data for the blockage effect.

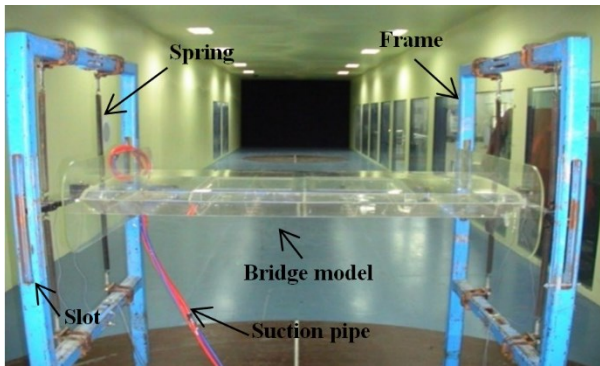
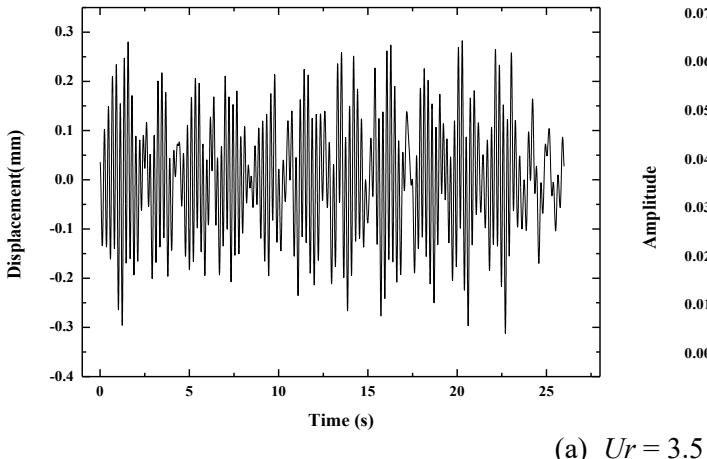


Figure 4. The experimental facility.

Four Type 4507B accelerometers were used simultaneously in this experiment.



The amplitude and phase frequency ranges of the accelerometers are 0.3 Hz - 6 kHz and 2 Hz - 5 kHz, respectively. They were fixed on the four corners in the bridge model, as shown in Fig. 5.

The acceleration measurements were obtained by acquiring data at a sampling frequency of 1000Hz for a period of 20 s.

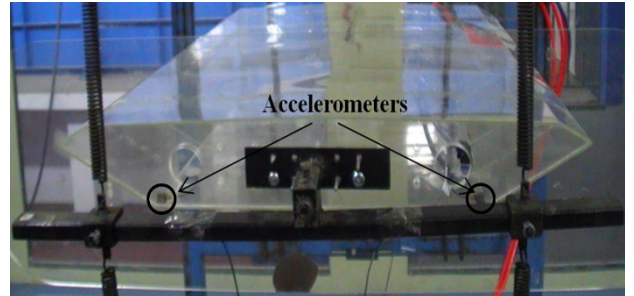


Figure 5. Accelerometers on the corners.

3 Experimental results and analysis

3.1 Without control

The time histories of vertical displacement and the frequency spectra of the bridge model are shown in Fig. 6. The reduced wind velocity is defined as $Ur = U / f_h D$, where f_h is the vertical natural frequency in still air ($f_h = 4.7$ Hz).

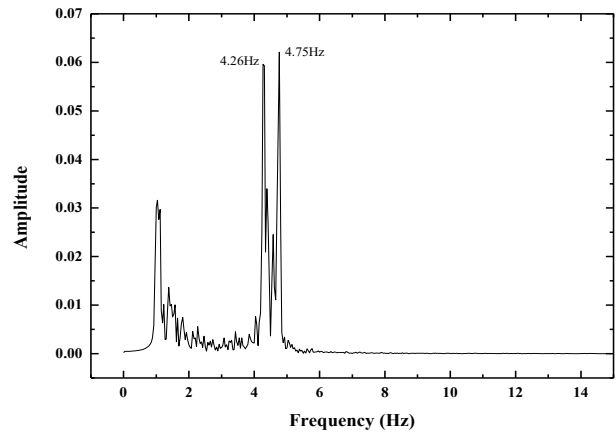


Figure 6. Time histories and frequency spectra of the vertical vibrations.

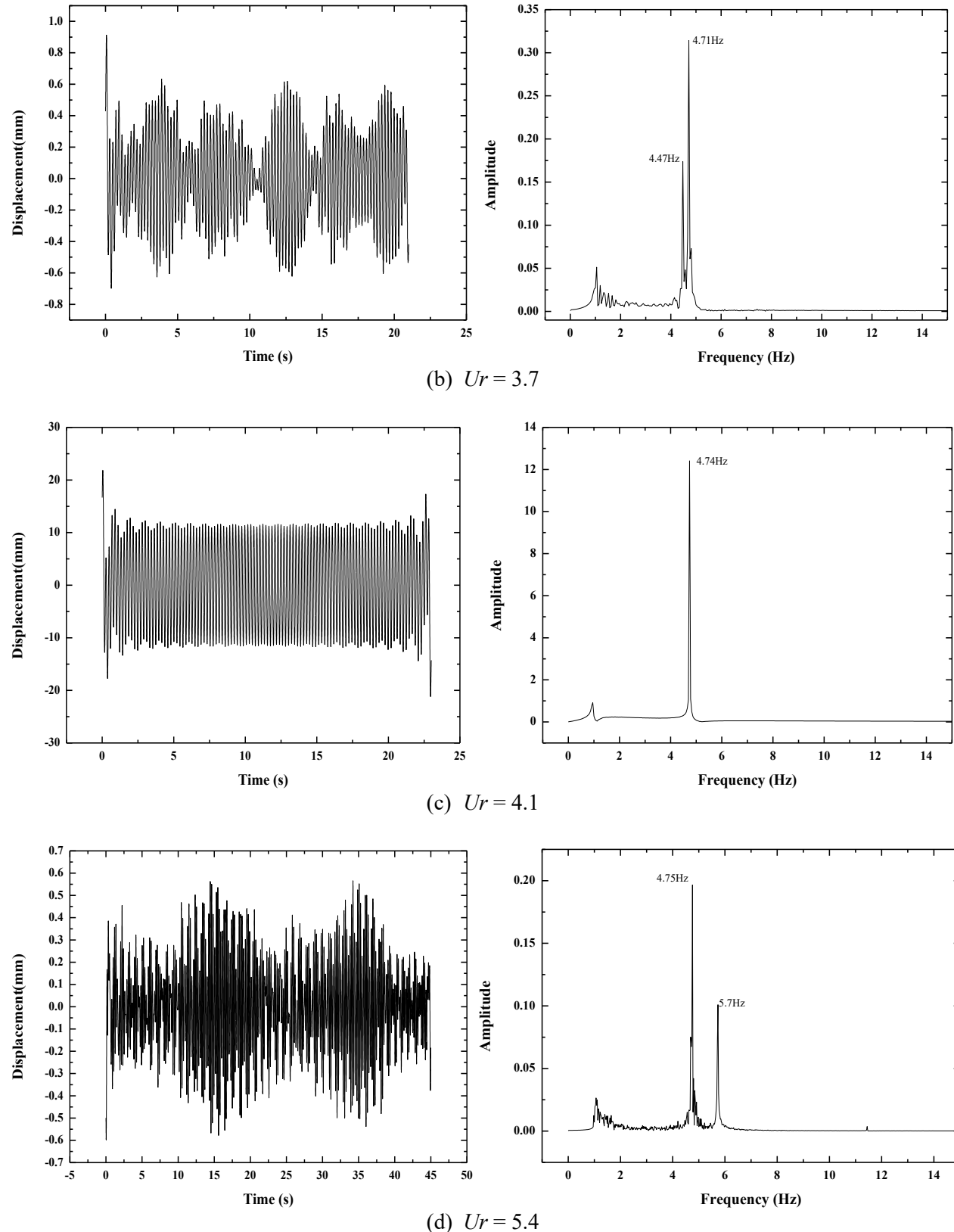


Figure 6. Time histories and frequency spectra of the vertical vibrations (continued).

Fig. 6 (a) shows that the critical reduced velocity of the vertical VIV is $U_r = 3.5$. The vortex shedding frequency ($f_v=4.26$ Hz) is very close to the vertical natural frequency. In Figs. 6 (b) and 6 (c), the predominant frequency is 4.7 Hz. In Fig. 6 (c), the vortex-shedding frequency is the same as the vertical natural frequency of the system. Therefore, the notable amplification of the magnitude is observed. As seen from Fig. 6 (d), there are two responses, 4.75 Hz and 5.7 Hz. The amplitudes of the vertical and torsional responses are shown in Fig. 7.

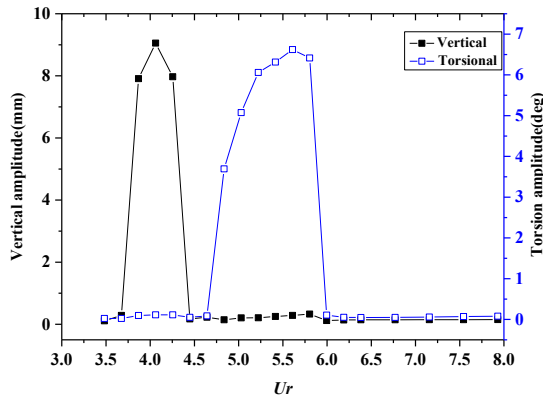


Figure 7. Amplitudes of the vertical and torsional responses.

In Fig. 7, the amplitude is found by measuring the root mean square value of response and multiplying by $\sqrt{2}$. The vertical VIV starts from $U_r = 3.5$ and ends at $U_r = 4.4$. The torsional VIV starts from $U_r = 4.6$, and ends at $U_r = 6.0$. At the reduced velocity at $U_r = 4.1$ and $U_r = 5.6$, the bridge model reaches its vertical and torsional maximum amplitude. The peak responses of vertical and torsional VIV are about 9 mm and 6.5°, respectively.

3.2 Controlled cases

In this experiment, the suction flow rate Q of every suction hole is 19 L/min. The vertical amplitudes of the model with or without suction control are shown in Fig. 8. By comparing the cases with no suction control and suction control, the seven suction configurations reduce the vertical amplitude of the model compared to the case with no suction. There are no significant differences among the K_1 to K_5 configurations. It is noteworthy that the effects of K_6 and the K_7 suction control configurations are remarkable, as they reduce the amplitudes of the model significantly during this experiment. The

torsional amplitudes of the model with or without suction control are shown in Fig. 9.

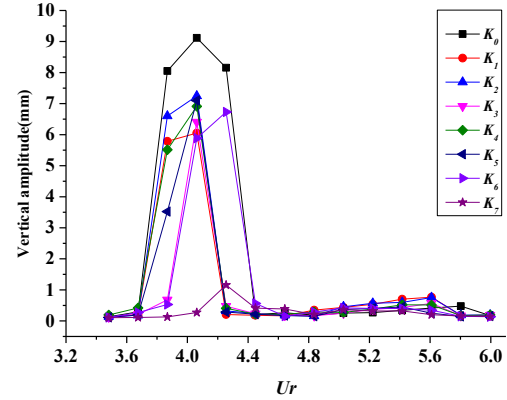


Figure 8. Amplitudes of vertical vibration.

In Fig. 9, by comparing the no suction and suction configurations, the effects of the seven suction configurations on reducing the torsional amplitude of the bridge model are better than no suction control.

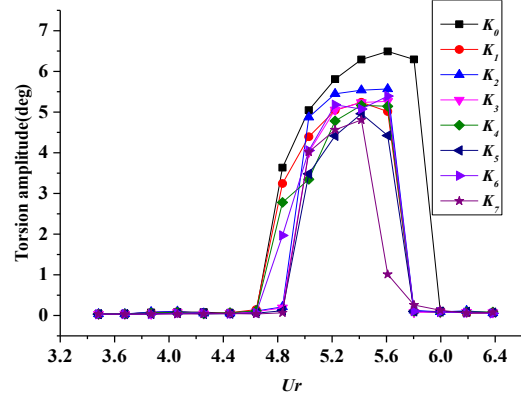


Figure 9. Amplitudes of torsional vibration.

The frequency ratio is defined as $f^* = f/f_h$, where f is the predominant vertical vibration frequency of the model. The frequency ratios of the model during this experiment are listed in Table 1.

Table 1 reveals that the vortex-induced vibration frequency of the bridge model with suction control increases slightly with the influence ratio approximately 1%. When the test is operated by the K_5 , K_6 and K_7 suction configurations, all of the frequency ratios increase to 1.01. The mass of the model is kept unchanged during the process in suction control. It is, therefore, believed that suction control does not change the frequency of the system. Therefore, suction control increases the effective damping of the system.

Table 1. Frequency ratio of the vertical vibration (f^*)

U_r	K	K_0	K_1	K_2	K_3	K_4	K_5	K_6	K_7
3.7	1	1	1	1	1	1	1.01	1.01	1.01
4.1	1	1.01	1	1	1	1	1.01	1.01	1.01
4.4	1	1.01	1.01	1.01	1.01	1	1.01	1.01	1.01

4 Numerical Simulation

4.1 Description of grid main

In this section, a two-dimensional bridge deck section model is used. And the grid system for the numerical simulation is shown in Fig. 10. The width and depth of the domain are 100D and 60D, respectively. The inflow boundary is specified with the inflow velocity. On the exit boundary, it is specified with free flow.

The upper and lower borders are specified with the wall. Navier-Stokes equations are solved by using finite volume method, second-order upwind difference form and the Semi-Implicit Method for Pressure-Linked Equations Consistent Algorithm [23]. The turbulence simulation is based on the Detached-Eddy Simulation [24]. The simulation is performed with ANSYS FLUENT [25]. To satisfy the Courant number condition, the time step is set at 10^{-4} s.

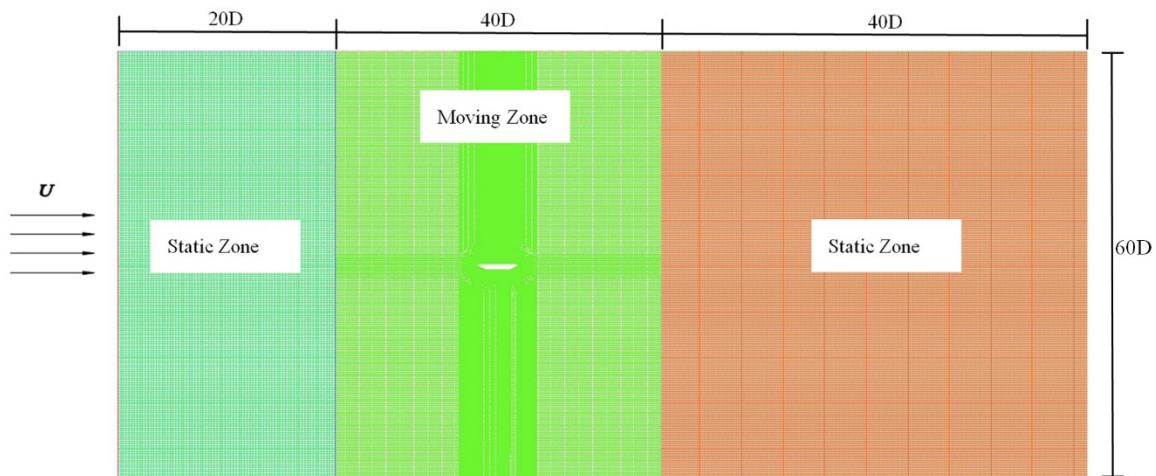


Figure 10. Computational domain of the bridge model.

In the simulation, three suction configurations, K_0 , K_4 and K_7 are chosen to study the flow characteristics affected by the suction control and the control mechanism, among which K_0 is chosen as the baseline case.

4.2 Suction condition

The suction hole can be simplified to a line with the length equal to the diameter of the suction hole ($r_s=7$ mm). The suction hole is assigned a velocity inlet boundary. The grids near the suction holes are densified, as shown in Fig. 11. A fine grid is created near the body and this grid becomes gradually coarser in the far field.

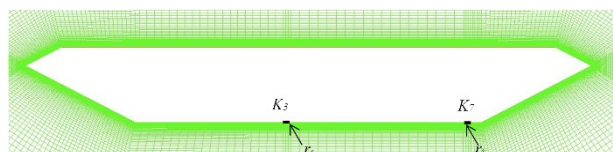


Figure 11. Meshes near the suction hole.

The suction velocity in the simulation (V_s) is calculated from Eq. (1).

$$\frac{V_s r_s}{D} = \frac{4\pi r_s^2 V}{DL} \quad (1)$$

According to Eq. (1), $V_s=0.53$ m/s.

4.3 Forced vibrations and frequency response of unsteady lift force

In this simulation, the model was subjected to a forced sinusoidal vibration,

$$h(t) = h_0 \cos \omega t \quad (2)$$

where, h_0 is amplitude of vibration, $h_0 = 1\text{cm}$; ω is the frequency of vibration, $\omega = 2\pi f_h = 9.4\pi$. $h(t)$ is considered positive along the positive y -direction. The dynamic mesh is subjected to vertical displacement obtained by the above expression. The frequency response part is expressed as follows:

$$C_L(t) = C_{L_0} \cos(\omega t + \beta) \quad (3)$$

where, $C_L(t)$ is the lift coefficient; C_{L_0} is the amplitude of the lift coefficient and β is the phase difference between the exciting force and the lift force acting on the surfaces. These can be obtained from the lift force history using numerical calculations as follows:

$$C_{L_0} = \sqrt{(a_m^2 + b_m^2)} \text{ and } \tan(\beta) = -b_m / a_m \quad (4a)$$

$$[a_m, b_m] = \frac{1}{T} \int_{-T}^T C_L(t) [\cos \omega t, \sin \omega t] \quad (4b)$$

The real and imaginary parts of the lift coefficients are determined using the following relations:

$$C_{LR} = C_{L_0} \cos(\beta), \quad C_{LI} = C_{L_0} \sin(\beta) \quad (5)$$

Details on this subject could be found in Sarwar et al. [26]. It is worth mentioning here that the system becomes unstable at a condition when $C_{LI} \geq 0$ indicating the negative aerodynamic damping region leading to a self-excited vibration of the system.

5 Numerical results and discussion

Fig. 12 shows the variation of the imaginary part of the lift coefficient that corresponds to the instability due to negative aerodynamic damping. In Fig. 12, without suction control, C_{LI} changes from negative to positive in the vicinity of $Ur = 3.4$. This indicates the presence of self-excited vibrations at about $Ur = 3.4$, called vortex-induced vibrations.

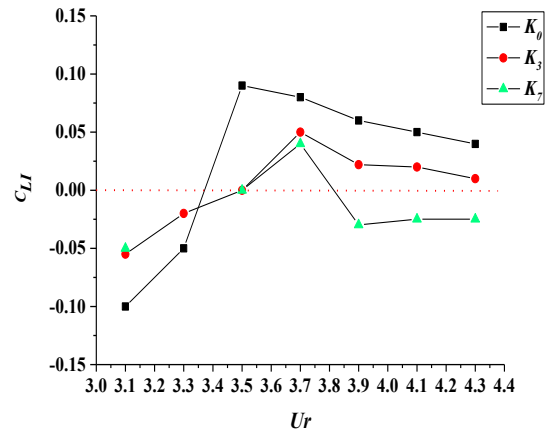


Figure 12. Imaginary part of lift coefficient.

The calculated result is consistent with the experiments. With the K_3 and K_7 configurations, the imaginary lift coefficients are about zero at $Ur = 3.5$, which means that the VIV critical reduced wind speed is around $Ur = 3.5$. When the reduced wind velocity range is $3.5 - 4.3$, the C_{LI} of the K_0 and K_3 configurations are positive, it means that they are in the aerodynamically unstable region. On the other hand, with the K_7 configuration, the C_{LI} is negative, except at $Ur = 3.7$. Therefore, the aerodynamic stability is the best with K_7 configuration. From Eq. (5), it can be concluded that suction control changes the phase difference between the exciting force and lift force acting on the surfaces of the model. Fig. 13 illustrates the streamlines of the time-averaged flow field.

In Fig. 13 (a), it is evident that the flow is separated on the lower side of the bridge model, and two large-scale vortices are near the trailing edge. In Fig. 13 (b), the two large scale vortices become smaller with the K_3 suction configuration. In Fig. 13 (c), under the influence of K_7 suction configuration the vortex almost disappears, as the suction control position is close to the separation region than in the K_3 suction configuration.

6 Conclusions

Using wind tunnel experiments, the efficiency of suction in suppressing the VIV of the bridge was studied. Based on the experiment, a computational fluid dynamics analysis was performed. The results allow the following conclusions to be drawn:

- (1) The suction control effectively suppresses the vortex-induced vibration of the bridge. It reduces the amplitude of vortex-induced amplitude. In addition,

the suction holes arranged on the surface near the leeward side of the model have the best result.

(2) The frequency of the vibration is increased with suction control in bridge model. The suction control especially operates near the leeward edge of the model bottom. It can be concluded that the effect of suction control on the VIV is attributable to the increase in the effective damping of the system.

(3) Suction control can increase the aerodynamic stability of the model by changing the phase difference between the exciting force and lift force acting on the surfaces of the model.

(4) Under the influence of suction control, the vortices near the trailing edge become smaller. The suction control performs well when the position of the control is close to the separation region.

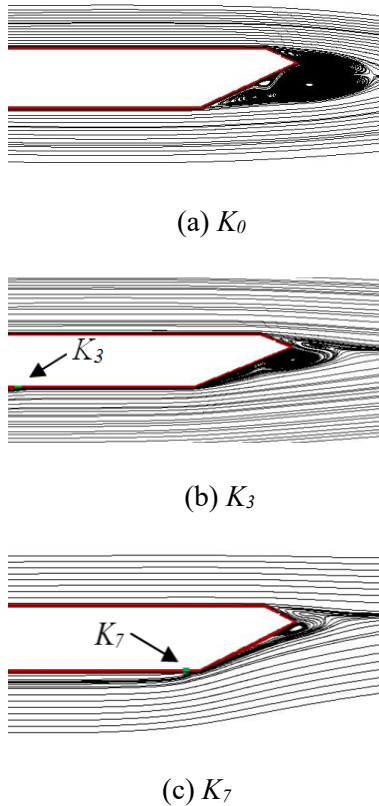


Figure 13. Streamlines of the time-averaged flow field ($Ur = 3.5$).

Conflict of interests

The authors declare that there is no conflict of interests regarding the publication of this paper.

Acknowledgments

The experimental work presented in this paper was conducted in The Joint Laboratory of Wind Tunnel and Wave Flume. Special thanks are conveyed to Professor BIAN Xiao-xian and Engineer ZHAO Peng for their help during the preparation of the test and for their efforts during the tests. We would like to show our deepest gratitude to Ms. Cho Mya Darli, Ms. Win Thi Yein and Professor ZHAN Jin-hui for their help.

References

- [1] Ceravolo, R., et al.: *Dynamic characterization of complex bridge structures with passive control systems*, Structural Control and Health Monitoring, 19 (2012), 4, 511–534.
- [2] Kim, S. J., et al.: *Operational field monitoring of interactive vortex-induced vibrations between two parallel cable-stayed bridges*, Journal of Wind Engineering and Industrial Aerodynamics, 123 (2013), 4, 143-154.
- [3] Mehmood, A., et al.: *Linear and nonlinear active feedback controls for vortex-induced vibrations of circular cylinders*, Journal of Vibration & Control, 20 (2014), 8, 1137-1147.
- [4] Belloli, M., et al.: *Force and wake analysis on a single circular cylinder subjected to vortex induced vibrations at high mass ratio and high Reynolds number*, Journal of Wind Engineering and Industrial Aerodynamics, 103 (2012), 1, 96-106.
- [5] Yeo, D., Jones, N.: *Computational study on aerodynamic mitigation of wind-induced, large-amplitude vibrations of stay cables with strakes*, Journal of Wind Engineering and Industrial Aerodynamics, 99 (2011), 4, 389-399.
- [6] Fujino, Y., Yoshida, Y.: *Wind-induced vibration and control of Trans-Tokyo Bay crossing bridge*, American Society of Civil Engineers, 128 (2014), 8, 1012-1025.
- [7] Larsen, A., et al.: *Storebælt suspension bridge – vortex shedding excitation and mitigation by guide vanes*, Journal of Wind Engineering and Industrial Aerodynamics, 88 (2000), 2, 283–296.
- [8] Hasheminejad, S. M., et al.: *Active vortex-induced vibration control of a circular cylinder at low Reynolds numbers using an adaptive fuzzy sliding mode controller*, Journal of Fluids and Structures, 50 (2014), 49-65.

- [9] Xu, K., Ge, Y., Zhang, D.: *Wake oscillator model for assessment of vortex-induced vibration of flexible structures under wind action*, Journal of Wind Engineering and Industrial Aerodynamics, 136 (2015), 1, 192–200.
- [10] Seo, J.-W., et al.: *Interference effect on vortex-induced vibration in a parallel twin cable-stayed bridge*, Journal of Wind Engineering and Industrial Aerodynamics, 116 (2013), 5, 7-20.
- [11] Kwok, K.C.S., et al.: *Wind-induced pressures around a sectional twin-deck bridge model: Effects of gap-width on the aerodynamic forces and vortex shedding mechanisms*, Journal of Wind Engineering and Industrial Aerodynamics, 110 (2012), 11, 50–61.
- [12] Li, Z.: *Tension control system design of a filament winding structure based on fuzzy neural network*, Engineering Review, 35 (2015), 1, 9–17.
- [13] Modi, V.J.: *Moving surface boundary-layer control: a review*, Journal of Fluids and Structures, 11 (1997), 6, 627-663.
- [14] Quadrante, L. A. R., Nishi, Y.: *Amplification/suppression of flow-induced motions of an elastically mounted circular cylinder by attaching tripping wires*, Journal of Fluids & Structures, 48 (2014), 7, 93-102.
- [15] Chen, W.L., et al.: *Suppression of vortex-induced vibration of a circular cylinder using suction-based flow control*, Journal of Fluids & Structures, 42 (2013), 4, 25-39.
- [16] Schlichting, H., Gersten, K.: *Boundary-layer theory*, McGraw-Hill, 1968.
- [17] Muralidharan, K., Patnaik, B. S. V.: *Control of vortex induced vibrations by suction and blowing*, American Physical Society, 2010.
- [18] Arcas, D., Redekopp, L.: *Aspects of wake vortex control through base blowing/suction*, Physics of Fluids, 16 (2004), 2, 452-456.
- [19] Chang, T. L., et al.: *Flow control of an airfoil via injection and suction*, Journal of Aircraft 46 (2009), 1, 291-300.
- [20] Xin, D., et al.: *Suppression method for wind-induced flutter of long-span bridge based on steady air-suction*, Journal of Jilin University (Engineering and Technology Edition), 41 (2011), 5, 1273-1278. (In Chinese)
- [21] Laima, S., et al.: *Investigation and control of vortex-induced vibration of twin box girders*, Journal of Fluids and Structures, 39 (2013), 5, 205-221.
- [22] Larsen A.: *Aerodynamic aspects of the final design of the 1624 m suspension bridge across the Great Belt*, Journal of Wind Engineering & Industrial Aerodynamics, 48 (1993), 2-3, 261–285.
- [23] Johansson, P., Davidson, L. M.: *Modified collocated SIMPLEC algorithm applied to buoyancy-affected turbulent flow using a multigrid solution procedure*, Numerical Heat Transfer, Part B: Fundamentals - An International Journal of Computation & Methodology, 28 (1995), 1, 39-57.
- [24] Spalart, P. R.: *Detached-eddy simulation*, Annual Review of Fluid Mechanics, 41 (2009), 1, 203-229.
- [25] Arslan, K.: *Three-Dimensional numerical investigation of turbulent flow and heat transfer inside a horizontal semi-circular cross-sectioned duct*, Thermal Science, 18 (2014), 4, 1145-1158.
- [26] Sarwar, M. W., et al.: *Prediction of unsteady lifts of oscillating rectangular cylinder at low reduced velocities by large eddy simulation*, The Sixth Asia-Pacific Conference on Wind Engineering, Seoul, Korea, 2005, 2476-2488.